NANO LETTERS

Letter

pubs.acs.org/NanoLett

Lipid Exchange Envelope Penetration (LEEP) of Nanoparticles for Plant Engineering: A Universal Localization Mechanism

Min Hao Wong,[†] Rahul P. Misra,[†] Juan P. Giraldo,[†,‡] Seon-Yeong Kwak,[†] Youngwoo Son,[†] Markita P. Landry,[†,§] James W. Swan,[†] Daniel Blankschtein,[†] and Michael S. Strano*[,†]

[†]Department of Chemical Engineering, Massachusetts Institute of Technology, Cambridge, Massachusetts 02139, United States

[‡]Department of Botany and Plant Sciences, University of California, Riverside, California 92521, United States

[§]Department of Chemical and Biomolecular Engineering, University of California, Berkeley, California 94720

Supporting Information

ABSTRACT: Nanoparticles offer clear advantages for both passive and active penetration into biologically important membranes. However, the uptake and localization mechanism of nanoparticles within living plants, plant cells, and organelles has yet to be elucidated.[1] Here, we examine the subcellular uptake and kinetic trapping of a wide range of nanoparticles for the first time, using the plant chloroplast as a model system, but validated in vivo in living plants. Confocal visible and near-infrared fluorescent microscopy and single particle tracking of gold-cysteine-AF405 (GNP-Cys-AF405), streptavidin-quantum dot (SA-QD), dextran and poly(acrylic acid) nanoceria, and various polymer-wrapped single-walled carbon nanotubes (SWCNTs), including lipid-PEG-SWCNT, chitosan-SWCNT and 30-base (dAdT) sequence of ssDNA $(AT)_{15}$ wrapped SWCNTs (hereafter referred to as ss$(AT)_{15}$-SWCNT), are used to demonstrate that particle size and the magnitude, but not the sign, of the zeta potential are key in determining whether a particle is spontaneously and kinetically trapped within the organelle, despite the negative zeta potential of the envelope. We develop a mathematical model of this lipid exchange envelope and penetration (LEEP) mechanism, which agrees well with observations of this size and zeta potential dependence. The theory predicts a critical particle size below which the mechanism fails at all zeta potentials, explaining why nanoparticles are critical for this process. LEEP constitutes a powerful particulate transport and localization mechanism for nanoparticles within the plant system.

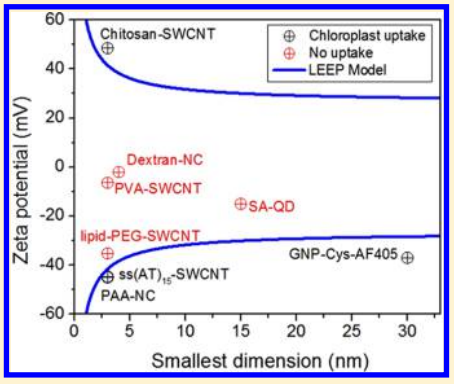

KEYWORDS: *Charge-mediated, nanoparticles, single-particle tracking, single-walled carbon nanotubes, chloroplast, LEEP (lipid exchange envelope and penetration)*

The incorporation of nanoparticles, such as nanotubes, nanowires, and quantum dots, into biological systems, particularly into mammalian cells and tissues, have enabled promising applications in drug delivery,[2−5] subcellular sensors,[6,7] and energy capture.[8] However, plant systems remain relatively unexplored due to complexities in uptake and localization pathways. In recent work,[9] we observed that nanoceria (NC), single-walled carbon nanotubes (SWCNTs) and conjugates of the two can traffic and localize within extracted chloroplasts, suggesting a universal mechanism. We have further designed nanoparticles that when infiltrated into the leaves of the plants enable unique and non-native functionalities such as light emission. In this work, we develop the theory behind this mechanism as a lipid exchange with the nanoparticle surface, allowing envelope penetration as the lipid exchange occurs onto the nanoparticle. This LEEP mechanism is then validated using microscopy and single-particle tracking of a wide range of nanoparticles, allowing one to design nanoparticles specifically for plant uptake.

In both in vitro and in vivo studies,[9] we showed that SWCNTs can utilize the LEEP mechanism that we elucidate to introduce non-native and unconventional functions in living plant systems, objectives that we term plant nanobionics. SWCNTs introduced into leaf tissue via vascular infiltration are found to localize in parenchyma tissues and subcellular organelles such as the chloroplasts and were found to significantly increase photosynthetic turnover and enable biochemical sensing from within the plant. SWCNTs coated with highly negative or positive surface coatings such as ss$(AT)_{15}$ and chitosan, respectively, are transported into and trapped inside intact chloroplasts. Interestingly, this does not occur when the SWCNTs are wrapped with polymers having more neutral zeta potential values. For example, both near-infrared (nIR) SWCNT fluorescent images and confocal three-dimensional (3D) mapping of the characteristic SWCNT Raman G-band (1580 nm) indicate that while ss$(AT)_{15}$-SWCNT are embedded within chloroplasts, lipid-wrapped SWCNTs do not interact with the lipid bilayer. To date, the

Received: November 2, 2015
Revised: January 6, 2016
Published: January 13, 2016

DOI: 10.1021/acs.nanolett.5b04467
Nano Lett. 2016, 16, 1161−1172

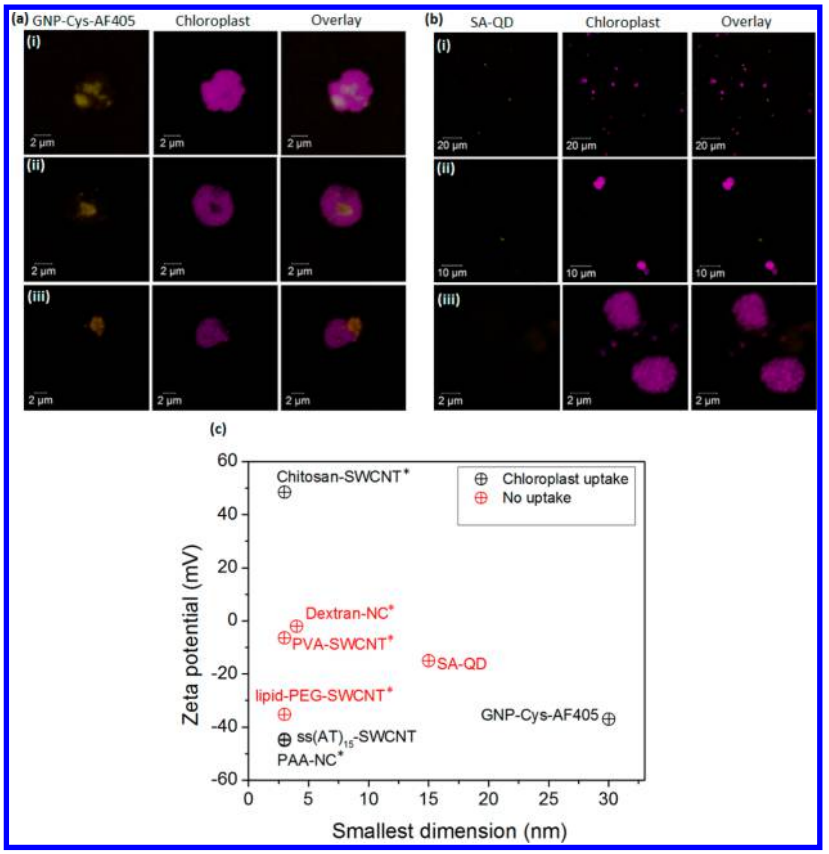

Figure 1. Entry of nanoparticles into the chloroplast is governed by surface charges and nanoparticle dimension. (a,b) Confocal micrographs of extracted chloroplasts incubated with GNP-Cys-AF405 and SA-QD at the end of 2 h of incubation. (a) (i–iii) Co-localization of GNP-Cys-AF405 within the chloroplasts. (b) (i–iii) No colocalization of SA-QD is observed. (c) Chloroplast uptake map showing successful nanoparticle uptake for chitosan-SWCNT, ss(AT)$_{15}$ SWCNT, GNP-Cys-AF405 and Polyacrylic acid-Nanoceria (PAA-NC) but not for Dextran-Nanoceria (Dextran-NC), poly(vinyl alcohol)-SWCNT (PAA-SWCNT), SA-QD, and lipid-polyethylene glycol-SWCNT (lipid-PEG-SWCNT). *Previously reported by Giraldo et al.[9]

transport mechanisms and distribution of nanoparticles into subcellular photosynthetic plant organelles like the chloroplast remain unknown. While several mechanisms, such as passive penetration,[10] endocytosis, and exocytosis[11−13] have been proposed and studied for nanoparticle entry into whole cells, the mechanism for nanoparticle uptake into subcellular organelles such as the chloroplast is currently unclear, motivating the present study.

The chloroplast is comprised of thylakoids contained within a double bilayer envelope.[14] The chloroplast is responsible for CO_2 reduction to valuable and energy rich sugars and sugar precursors and as such has been extensively studied due to the potential to exploit plastome (genetic material of plastids) engineering for biotechnological applications,[15−17] as well as the potential for the chloroplast to serve as an engineering material.[18] Chloroplasts are similar to Gram-negative bacteria and mitochondria in that they are surrounded by two membranes, an outer membrane and an inner membrane.[19] Glycerolipids (galactolipids and sulfolipids) account for 52% of the total lipids in the outer membrane, while the inner membrane contains nearly 85% of glycerolipids such as Monogalactosyldiacylglycerol.[20] The presence of sulfolipid and phospholipid confers a net negative charge to the chloroplast membrane surface,[14] leading one to hypothesize that positively charged nanoparticles have a natural affinity for chloroplast localization with the opposite being true for negatively charged nanoparticles. However, our observations and modeling presented in this work fundamentally contradict this hypothesis, as demonstrated below. The smooth outer membrane of the envelope is more permeable than the inner membrane[21] and contains porins that allow passage of some ionic compounds and small molecules. However, the diameters of chloroplast porins are calculated to be 2.5−3.0 nm,[22] which is unlikely to permit the rapid nanoparticle entry studied in this work. Furthermore, the inner membrane is known to be impermeable to most ions and metabolites,[22] which renders the observed ability of charged nanoparticles to traffic into the chloroplast surprising. Significant interest lies in understanding the uptake of biological molecules such as DNA and plasmids into chloroplasts due to their potential for gene transfer[23] and plant synthetic biology. For example, the forced uptake of DNA into chloroplast plastids by biolistic means has been studied extensively[4,5] but remains poorly understood,[24] although mechanisms such as DNA penetration of the chloroplast envelope,[24] transient alteration of envelope permeability, or the formation of temporal holes in membrane structures[25] have been suggested.

Imaging and tracking single nanoparticles as they traffic through cellular space can provide valuable information on various important biological mechanisms. Here we employ confocal microscopy on isolated chloroplasts to study the effect of surface charges of various nanoparticles on chloroplast entry. We further employ high-resolution single particle tracking to study the uptake and kinetic trapping of ss(AT)$_{15}$-wrapped

DOI: 10.1021/acs.nanolett.5b04467
Nano Lett. 2016, 16, 1161−1172

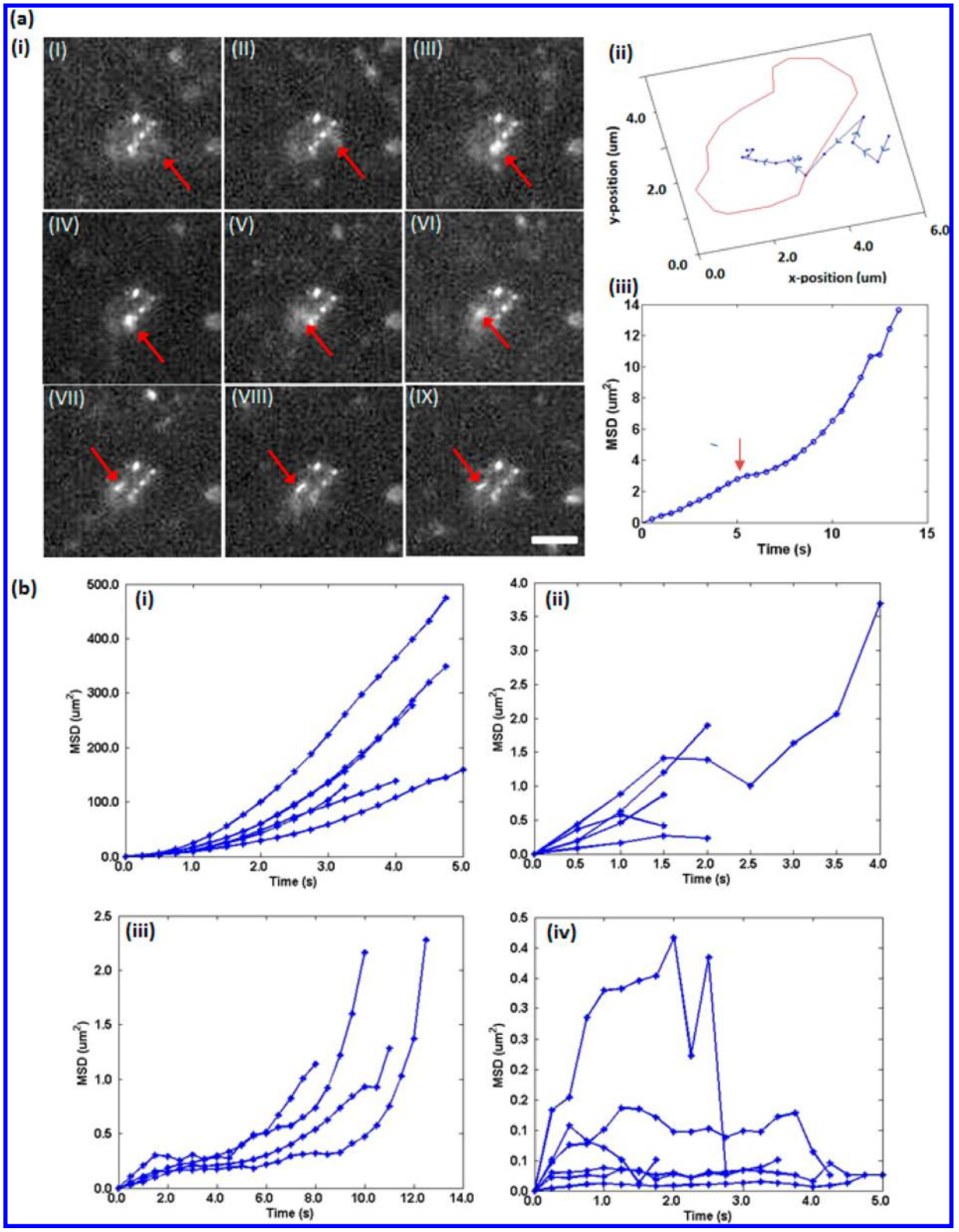

Figure 2. Representative figures showing entry and trapping of SWCNTs via LEEP mechanism. (a) (i) Single-particle tracking of SWCNTs using their intrinsic fluorescence under 785 nm excitation (fluorescence seen by the bright spots) allows the movement of individual SWCNTs to be tracked as they enter the chloroplast (tracked SWCNT represented by the red arrow with images labeled (I–IX), and x–y graph tracing the location of this particle is shown in (ii)). (iii) MSD shows the transition of the SWCNTs from outside the chloroplast to within (labeled by the red arrow), indicated by the change in gradient of the MSD plot (which can be correlated to a difference in diffusivity). Scale bar = 5 μm. (b) The motions of SWCNTs can be described as a series of distinct transport steps: (i) Convective diffusion outside the chloroplast as indicated by the distinctive quadratic curve. (ii) Transport across the chloroplast bilayer membrane (where nanoparticles are confined temporally on the membrane surface as indicated by the relatively small MSD values). (iii) Transport from the membrane to within the chloroplast (assigned as confined to convective). (iv) Kinetic trapping of SWCNTs within the interior of the chloroplast (represented by almost constant MSD values).

DOI: 10.1021/acs.nanolett.5b04467
Nano Lett. 2016, 16, 1161–1172

nanotubes (taken as a model nanoparticle) as they enter the chloroplast. Mathematical analysis of the experimental in vitro trajectories is used to describe the mechanistic steps involved in SWCNT uptake and accumulation into the chloroplast. We utilized mean-squared displacement (MSD) analysis to model segments of particle motion to elucidate mechanisms of SWCNT transport into plastids. After quantifying the translational characteristics of SWCNTs as a function of viscosity, we used the SWCNT diffusivities to compute the probable SWCNT lengths that were found to transport into the chloroplasts. Post-internalization, SWCNTs demonstrated confined diffusion, convective diffusion, and were confirmed to be kinetically trapped.

The observed kinetic trapping and penetration of nanoparticles into chloroplast can be explained by a mathematical model that we have termed the lipid exchange envelope and penetration model (LEEP). In the LEEP model, interactions between charged nanoparticles and the surface charges on the chloroplast membrane are assumed to soften the membrane, leading to an expanded and fluid state. This process is assumed to be favored thermodynamically and allows the nanoparticles to penetrate into the chloroplast. Glycerolipids, which comprise the majority of the chloroplast membranes are then assumed to chemically interact with the charged nanoparticles as they transport across the chloroplast membrane. The lipid-wrapped nanoparticles then diffuse into the chloroplast, before being trapped irreversibly in the interior. Kinetically trapped nanoparticles are unable to transport out of the chloroplast, and the chloroplast membrane reheals.

To study the effect of surface charges of the nanoparticles on their entry into chloroplasts isolated chloroplasts were first obtained from commercially procured baby spinach leaves (*Spinacia oleracea*) using protocols modified from Weise et al.[26] ss(AT)$_{15}$-SWCNT (3 nm diameter and zeta potential of approximately −45 mV) were prepared by tip sonication of ss(AT)$_{15}$ with HiPCO SWCNTs (Unidym) in a 2:1 wt ratio (see SI for details). Gold-cysteine-AF405 nanoparticles (GNP-Cys-AF405) (30 nm diameter and zeta potential of ∼ −38 mV) were prepared using gold nanoparticles purchased from Nanocomposix. L-cysteine (Sigma-Aldrich, MW. 121.16, 0.023 mg, 19 μM, 1 equiv) was reacted with Alexa fluor 405-NHS (Life science, MW 1028.3, 0.2 mg, 19 μM, 1 equiv) in 400 μL of phosphate-buffered saline (pH 7) for 1 h at room temperature. Two milliliters of gold nanoparticles were then mixed with cysteine-Alexa Fluor 405 conjugates for 2−3 h at room temperature. Streptavidin-quantum dots (SA-QD) were used as purchased. Nanoparticles were characterized by direct light scattering (DLS) and phase analysis light scattering zeta potential analyzer (PALS) (see Experimental Details in SI for details). The nanoparticles were then incubated with the chloroplast for 2 h before analysis with confocal microscopy or nIR microscopy (in the case of SWCNT nanoparticles) to determine if nanoparticles were localized within the chloroplasts.

Irreversible Trapping of Nanoparticles into Chloroplasts. The uptake of nanoparticles into the chloroplast was only observed for nanoparticles with high surface charge. This was true of both positively and negatively charged nanoparticles. Highly charged nanoparticles such as cysteine-gold nanoparticles (−38 mV) (Figure 1a) and ss(AT)$_{15}$-SWCNT (Figure 2a and Supporting Information (SI) Figures S1 and S2) that entered the chloroplast were further found to be irreversibly trapped (Figure 1a). More neutrally charged nanoparticles such as SA-QD (−15 mV) were found unable to penetrate into the chloroplast interior (Figure 1b). The correlation of nanoparticle surface charges (zeta potentials) and the ability to penetrate the chloroplast is seen in Figure 1c, where nanoparticles with zeta potential magnitudes higher than 30−40 mV were demonstrably trapped within the chloroplast. More neutrally charged nanoparticles, including dextran-nanoceria (−2 mV) and PVA-SWCNT (−6.4 mV), were not found within the chloroplast interior.

Single-Particle Tracking of SWCNTs into Chloroplasts. The mechanism of nanoparticle entry was studied via single-particle tracking of SWCNT intrinsic photoluminescence. ss(AT)$_{15}$-SWCNTs were used as model nanoparticles. The isolated chloroplast suspension was placed on a microscope slide and covered with a glass coverslip. The intactness of the chloroplasts can be confirmed from bright-field images (SI Figure S1) as seen from the distinctive halo around intact chloroplast membranes.[27] The depth of field for the experiment can be calculated using the equation given by Shillaber, eq 1

$$d = \frac{(\lambda)(\sqrt{n^2 - (\mathrm{NA})^2})}{(\mathrm{NA})^2} \quad (1)$$

where λ is the wavelength (HiPCO SWCNT (as purchased from Unidym) ∼ 1000 nm), n is the refractive index (oil = 1.515), and NA is the objective numerical aperture (1.46). The depth of field was determined to be approximately 190 nm.

One microliter of 10 mg/L ss(AT)$_{15}$-SWCNT (SWCNT preparation details given in SI) was introduced at the edge of the microscope coverslip, allowing the passive convection and Brownian diffusion of ss(AT)$_{15}$-SWCNTs across the microscope coverslip. As the ss(AT)$_{15}$-SWCNTs comes into contact with the chloroplasts, the fluorescence of ss(AT)$_{15}$-SWCNTs was visualized with a laser excitation (785 nm) off-resonance to photosynthetic pigments. ss(AT)$_{15}$-SWCNTs were found to localize within the chloroplast (images given in SI, Figures S1 and S2). The increase in normalized intensity over a 400 s period, measured from the time when the SWCNTs were first introduced shows the continual uptake and irreversible trapping of SWCNTs in the chloroplast. Using a lower concentration of 5 mg/L ss(AT)$_{15}$-SWCNTs allowed single particle tracking of SWNCTs as they passively transported across the chloroplast double membrane into the plastid interior.

Using nIR fluorescent microscopy, individual SWCNTs were tracked with an exposure time of 0.5 s as they diffused from outside the chloroplast and across the chloroplast envelopes to the plastid interior. The time-lapsed images shown in Figure 2a(i) provide the first conclusive proof of the entry and subsequent kinetic trapping of individual SWCNTs as they traversed into the chloroplast (SI movie M1).

The use of single-particle tracking of SWCNT trajectories allows the complete pathway of the LEEP process to be described as a series of distinct and sequential transport steps, convection and diffusion outside the chloroplast, confined to convective transport across the membrane, confined diffusion within the chloroplast, and kinetic trapping within the chloroplast interior. By converting the images into quantitative values using image processing, MSD values for each step were used to model segments of particle motion to piece together mechanisms of incorporation. MSDs were calculated using the equation proposed by Jin and Verkman[28] and shown in eq 2

DOI: 10.1021/acs.nanolett.5b04467
Nano Lett. 2016, 16, 1161−1172

$$\mathrm{MSD}(n\Delta t) = \frac{1}{N-1-n}\sum_{j=1}^{N-1-n}[x(j\Delta t + n\Delta t) - x(j\Delta t)]^2 + [y(j\Delta t + n\Delta t) - y(j\Delta t)]^2 \quad (2)$$

where x is the x-coordinate, y is the y-coordinate, and Δt is the lag time. The complete transport mechanism of SWCNTs into chloroplasts is described by analysis of the different segments of particle motion. Each step is observed to recur throughout the various experiments. SWCNTs were found to undergo convective diffusion outside of the chloroplast, as described by the distinctive quadratic function shown in eq 3

$$\mathrm{MSD}_{\mathrm{convective}} = 4D_0 t + (Vt)^2 \quad (3)$$

where D_0 is the diffusion coefficient, V is the velocity, and t is the time step. They are then internalized and transported into the chloroplast via confined and convective transport (Figure 2b(ii,iii)), where they finally reach a kinetically trapped state (Figure 2b(iv)). Trapped SWCNTs were observed to remain within the chloroplasts for durations that are far greater than the time required for membrane penetration with negligible MSD values at all time lags.

The MSD curves can be statistically regressed as a quadratic function (eq 3) for convective transport with a diffusive component. Using the two-dimensional diffusivities obtained from fitting of the MSD curves, the lengths of SWCNTs found to enter the chloroplast via LEEP were calculated using an equation proposed by Marshall et al. and Li et al.[29,30] (eq 4) to describe the two-dimensional translational diffusion coefficient of a rodlike macromolecule in an unbounded fluid

$$D_0 = \frac{k_B T}{8\pi\eta_m L}\left[3\ln\left(\frac{L}{D}\right) + 2A + B\right] \quad (4)$$

where L is the length of the SWCNT, D is the diameter of the SWCNT (taken to be 3 nm as validated by atomic force microscopy (AFM), Supporting Information, Figure S3), $A = -0.114$, $B = 0.886$ for $\frac{L}{D} \to \infty$ (which is valid for the SWCNTs studied), and η_m is the viscosity of the medium (9.3 cP).[31] The range of probable SWCNT lengths calculated compared well with the observations of ss(AT)$_{15}$-SWCNTs seen under AFM analysis (SI Figure S3). Correlations were drawn between the SWCNT length and three different measured parameters, the membrane barrier crossing velocity, the stopping distance (the distance traveled from the membrane into the chloroplast before kinetic trapping), and the time taken for kinetic trapping measured from the time when the SWCNT first enters the chloroplast. We note that there was no clear length dependence observed (SI Figures S4 and S5) to the physical parameters.

The penetration of charged particles across cell membranes is a subject investigated in several previous studies, most of which focus on cell internalization. While the findings of several studies differ based on the experimental or simulation conditions used, it is generally thought that cationic particles are able to electrostatically bind to negatively charged groups on the cell surface and translocate across the membrane, whereas negative or neutral particles interact minimally with the cell surface.[32] Simulation studies[33] have shown that cationic nanoparticles can penetrate across the cell membranes passively. Experimentally, several authors have demonstrated the pore-forming propensity of cationic particles on cell membranes.[34−36] Interestingly, hole formation in lipid bilayers by cationic particles is a common outcome, regardless of chemical composition or nanoparticle shape. However, particularly for the chloroplast plastid, genetic transformation of the plant remains difficult due to the inability of many nanoparticles to cross the double bilayer membrane of the chloroplast. The transport of proteins into chloroplasts via active pathways requires specific receptor families depending on protein type,[37] while free DNA and other foreign proteins are unable to cross the chloroplast membrane boundary. While the charge-mediated entry described in our study involves experimental conditions and corresponding entry mechanisms that are different from those of other authors, the ability of charged particles to easily penetrate into the negatively charged chloroplast membrane, especially for anionic nanoparticles, is a surprising result that cannot be readily explained by existing models and experimental results.

Mathematical Formulation of the LEEP Model. We have developed a mathematical model to explain the LEEP mechanism. The model is developed in accordance to four distinct steps:

Step 1: Ion-Induced Potential around the Charged Nanoparticle. A charged nanoparticle in the presence of free ions in an electrolyte solution attracts counterions from the solution leading to the formation of a counterion cloud around the nanoparticle. The thickness of the counterion cloud depends on the ionic strength of the solution and in principle, decreases with higher ionic strength. The formation of this counterion cloud, also called the electric double layer, leads to the screening of the surface charge on the nanoparticles. We will model the electric double layer around the charged nanoparticle by incorporating image charge effects into the mean-field Poisson−Boltzmann (PB) model. The PB model assumes point-sized ions and solvent molecules, constant dielectric permittivity of the medium, and neglects ion−ion correlations. We further assume a spherical geometry for the nanoparticle, which is the case for many of the nanoparticles studied here, such as SA-QD, nanoceria, and GNP-Cys-AF405.

The PB model for a spherical nanoparticle is expressed as follows:[38]

$$\frac{1}{r^2}\frac{\mathrm{d}}{\mathrm{d}r}\left(r^2\frac{\mathrm{d}\psi}{\mathrm{d}r}\right) = \frac{-\sum z_i e c_{i0} e^{-z_i e\psi/k_B T}}{\epsilon_w \epsilon_0} \quad (5)$$

where c_{i0} and z_i are the concentration and valence of species i, respectively, ψ is the electrostatic potential at a radial distance r from the center of the charged nanoparticle, e is the electronic charge, ϵ_W is the dielectric permittivity of the medium (ϵ_W = 80), ϵ_0 is the dielectric permittivity of vacuum, k_B is the Boltzmann constant, and T is the absolute temperature (taken to be 300 K). In the Debye−Huckel (DH) approximation, where $\frac{z_i e\psi}{k_B T} < < 1$, eq 5 can be linearized to obtain the following equation

$$\frac{1}{r^2}\frac{\mathrm{d}}{\mathrm{d}r}\left(r^2\frac{\mathrm{d}\psi}{\mathrm{d}r}\right) = \kappa^2\psi \quad (6)$$

where $\kappa^2 = \sum \frac{(z_i e)^2 c_{i0}}{\epsilon_w \epsilon_0 k_B T}$, κ^{-1} is the Debye−Huckel screening length (the thickness of the electrical double layer in the DH approximation). Equation 6 can be solved with the following two boundary conditions: (1) $r = a$, $\psi = \xi$ (a is the radius of the charged nanoparticle and ξ is the electrostatic potential on the nanoparticle surface) and (2) $r \to \infty$, $\psi \to 0$ to yield the

DOI: 10.1021/acs.nanolett.5b04467
Nano Lett. 2016, 16, 1161−1172

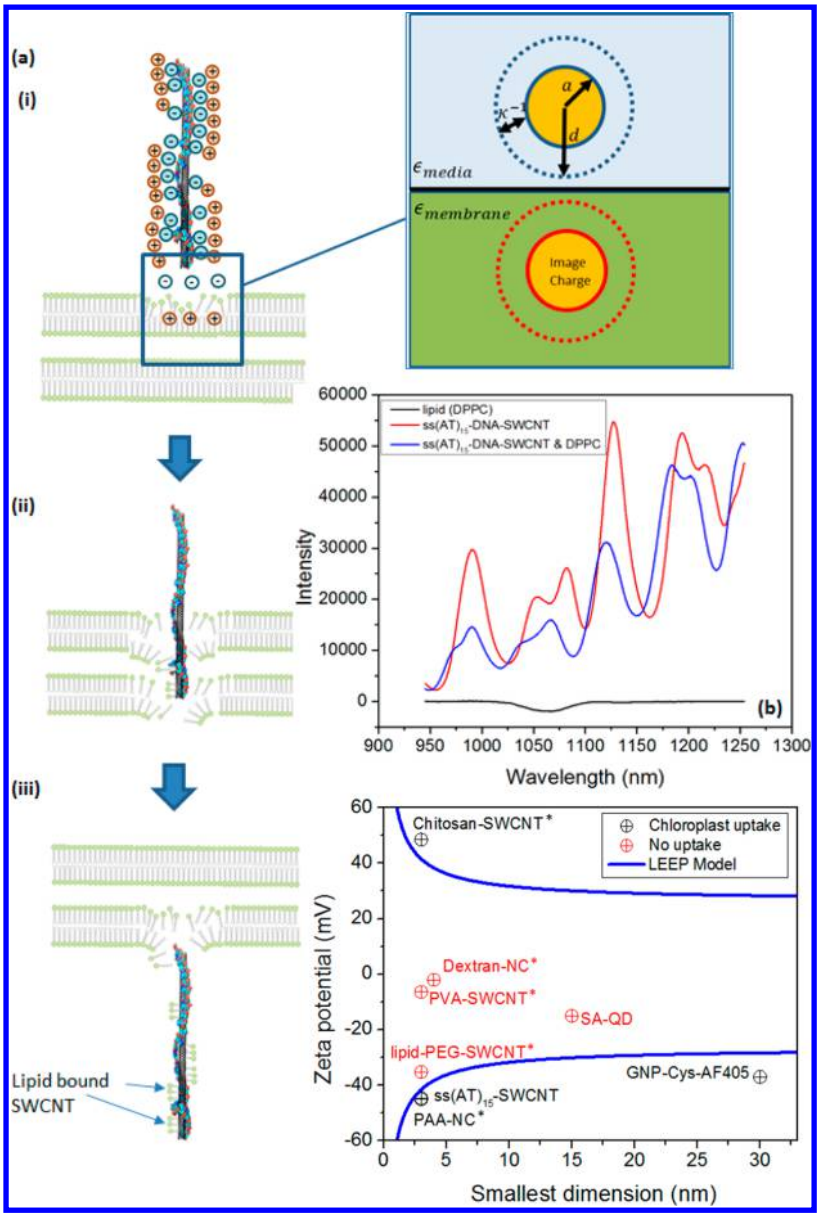

Figure 3. LEEP of nanoparticles into chloroplasts. (a) (i) Nanoparticles with high zeta potential ($ss(AT)_{15}$ SWCNT shown here) approache the chloroplast outer membrane that is similarly negatively charged. This induces image charges on the lipid bilayer (indicated by the blue box and cartoon depiction) and leads to membrane expansion and softening. (ii) Glycerolipids wrap around $ss(AT)_{15}$ bound SWCNT as they interact with the membrane. Interaction between lipids and $ss(AT)_{15}$ SWCNT is confirmed by the solvochromatic shift observed upon addition of dipalmitoylphosphatidylcholine (DPPC) to $ss(AT)_{15}$ SWCNT. (iii) The lipid bound $ss(AT)_{15}$ SWCNT enters the chloroplast and binds to the chloroplast interior. The lipid membrane of the chloroplast reheals. (b) Solvatochromic shift and intensity attenuation is observed upon addition of DPPC to $ss(AT)_{15}$-SWCNT. (c) LEEP model applied to chloroplasts (with ϵ_M = 2.2) as indicated by blue lines and is shown together with experimental data presented in Figure 1c.

following result for the electric potential profile around the nanoparticle[39]

$$\psi = \frac{\xi a e^{-\kappa(r-a)}}{r} \tag{7}$$

Although the DH approximation is generally valid for zeta potentials smaller than 25.7 mV in the case of monovalent electrolytes at room temperature, we found from our numerical solution of eq 5 that the DH approximation in eq 6 overestimates the electrostatic potential by a maximum of 20% for zeta potential equal to 60 mV, which is the highest value of zeta potential used for the purpose of modeling the electric double layer in our study (Figure S6 (Supporting Information)). This makes the DH approximation reasonable for the rest of our analysis of the electric double layer.

Step 2: Lipid Membrane Softening. Because the dielectric constant of the chloroplast double bilayer ($\epsilon_{Membrane} = \epsilon_M$ = 2.2)[40] is different from that of the medium surrounding the nanoparticles (ϵ_{water}), the charged nanoparticle will induce a potential drop across the lipid membrane. The surface potential at the membrane surface can be calculated by considering a fictitious image of the charged nanoparticle inside the lipid membrane. This fictitious charge is considered to be within the lipid membrane in order to correctly reproduce the boundary conditions for the electric field at the interface between the medium surrounding the nanoparticles and the lipid mem-

DOI: 10.1021/acs.nanolett.5b04467
Nano Lett. 2016, 16, 1161−1172

brane. The surface potential of the fictitious image charge inside the lipid membrane is given by[41]

$$\xi_{\text{image}} = \left(\frac{\epsilon_w - \epsilon_M}{\epsilon_w + \epsilon_M}\right)\xi \tag{8}$$

where ξ_{image} is the surface potential of the fictitious image charge inside the lipid membrane. Equation 8 shows that when $\epsilon_M = \infty$ (i.e., for a metal), $\xi_{\text{image}} = -\xi$. However, for an interface between two dielectric media the magnitude as well as the sign of the surface potential of the fictitious image charge depends on the dielectric constants of both media. Although the charged nanoparticle induces a transmembrane potential drop that eases pore formation in the lipid membrane, we assume that the electric field around the charged nanoparticle remains unperturbed by the pore formation process, that is, we neglect any changes in the electrostatic potential distribution resulting from the mechanical rupture of the pore. This is valid if we assume that the pore formation process does not lead to any significant change in the dielectric constant of the lipid membrane, which is a generally valid initial guess for the mean-field theory of an electric double layer. We also neglect image charge contributions from the counterions comprising the electric double layer around the nanoparticle. Following the approach used by Onsager and Samaras,[42] the electrostatic potential at any point is determined by the superposition of the electrostatic potential resulting from the charged nanoparticle and the electrostatic potential resulting from the fictitious image charge. Using eqs 7 and 8, the expression for the electrostatic potential around the charged nanoparticle in the vicinity of the lipid membrane is given by

$$\psi = \frac{\xi a e^{-\kappa(r_1 - a)}}{r_1} + \left(\frac{\epsilon_w - \epsilon_M}{\epsilon_w + \epsilon_M}\right)\frac{\xi a e^{-\kappa(r_2 - a)}}{r_2} \tag{9}$$

where a is the radius of the nanoparticle, and r_1 and r_2 are radial distances from the center of the nanoparticle and the image charge, respectively, (see Figure 3). Equation 9 shows that because $\epsilon_w > \epsilon_M$ in our case, the contribution to the electrostatic potential from the image charge (second term on the right side of eq 9) has the same sign as that of the contribution from the charged nanoparticle (first term on the right side of eq 9). As a result, the electrostatic potential at any point is enhanced due to the presence of the lipid membrane having a lower dielectric constant than the surrounding medium (water). At the lipid membrane surface, $r_1 = r_2 = d$, which results in the following relation between the induced electric potential, V, and the nanoparticle surface potential, ξ

$$V = \left(\frac{2\epsilon_w}{\epsilon_w + \epsilon_M}\right)\left[\frac{\xi a e^{-\kappa(d - a)}}{d}\right] \tag{10}$$

Step 3: Lipid Exchange. As the charged nanoparticle approaches the chloroplast, lipids from the softened membrane transfer to the charged nanoparticle surface, facilitated by the fact that lipids are zwitterionic and can therefore establish specific enthalpic interactions with either positively charged or negatively charged nanoparticles. Intensity attenuation and the solvatochromic shift of SWCNT nIR fluorescent peaks are observed upon lipid addition to ss(AT)$_{15}$-SWCNTs, indicating that lipids are able to chemically interact with and bind to nanoparticles. This interaction is further confirmed by a red shift in absorbance spectra (SI Figure S7), which indicates larger surface exposure to water molecules of the underlying SWNT and a less tightly bound corona. This indicates that the lipid molecules interact with the DNA corona phase and change the local dielectric environment, by adsorbing onto the SWNT surface and possibly exchanging segments of the original DNA wrapping.[43] The attraction of lipids (in the softened membrane) with the nearby nanoparticles creates a driving force to translate the nanoparticles inward through the membrane. The interactions of charged polymers with zwitterionic lipids have been well studied by several authors. Sikor and coauthors[44] reported that the polar head groups of 1,2-dimyristoyl-*sn*-glycero-3-phosphocholine (DMPC) are zwitterionic and small values of the zeta potential have been measured by electrophoresis for unilamellar DMPC vesicles.[45] They further found that at suitable salt concentrations, charged polymers (polyethyleneamine) are adsorbed onto the surface of DMPC vesicles. Similarly, Langecker and co-workers[46] specifically studied DNA–lipid interactions and how DNA nanostructures can either remain mobile on membranes or can be embedded within lipid bilayers. Interestingly, Bo and co-workers[47] also found via fluorescence and calorimetry methods that the local phase state of phospholipid bilayers can be switched by binding of charged nanoparticles such that they alter the tilt angle of the phosphocholine. In their work, they excluded the traditional explanation of spatial patchiness, based on specific binding, by constructing phospholipid membranes comprised of a sole lipid type. The possibility of specific binding was eliminated by selecting lipids bearing phosphocholine head groups, which are uncharged under the buffer conditions used in their experiments. We have mathematically described this nanoparticle–lipid interaction using a site balance (eq 11)

$$\theta_i + L_i \rightleftharpoons L_i\theta_i \tag{11}$$

where θ_i denotes the concentration of free sites on the nanoparticle surface, and L_i represents the concentration of membrane lipids interacting with the charged nanoparticle. The induced electric potential and nanoparticle–lipid interaction provide the energetic contribution required for the formation of pores in the chloroplast membrane, which can be defined as the pore formation energy, W_p, described by eq 12[48,49]

$$W_p = -\pi R_p^2\gamma + 2\pi R_p\Gamma + \Delta\Delta H(4\pi R_p^2\rho_n) \tag{12}$$

where γ is the membrane tension, Γ is the line tension of the pore, R_p is the pore size, ρ_n is the lipid density on the nanoparticle, and $\Delta\Delta H = \Delta H_{L_i\theta_i} - \Delta H_{f\theta_i} - \Delta H_{fL_i}$, where $\Delta H_{L_i\theta_i}$, $\Delta H_{f\theta_i}$, and ΔH_{fL_i} are the free energy of the lipid-nanoparticle, nanoparticle binding sites, and membrane lipids, respectively. The magnitude of $\Delta\Delta H$ can be estimated to be approximately 0.05 k_BT/per lipid bound.[47,50] The first term in eq 12 represents the decrease in surface energy of the lipid membrane associated with the formation of the pore, the second term represents an increase in energy because of line tension at the edge of the pore, and the last term is the net enthalpic contribution to the pore formation energy resulting from the lipids transferring from the lipid membrane onto the nanoparticle surface. $\Delta\Delta H$ quantifies the heat of reaction per lipid transferring to the nanoparticle surface, as described by eq 11. The chloroplast can be modeled as a lipid vesicle with a membrane tension γ_0 of approximately 10^{-3}–10^{-4} Nm^{-1}.[51] When the charged nanoparticle approaches the lipid membrane, it induces a transmembrane potential drop across the lipid bilayer as described by eq 10. The induced potential drop

DOI: 10.1021/acs.nanolett.5b04467
Nano Lett. 2016, 16, 1161–1172

tends to lower the stability of the membrane against thermal fluctuations. We model this electrostatic contribution to the surface energy by treating the lipid bilayer as a simple parallel plate capacitor and include the energy of the parallel plate capacitor in the expression of the membrane tension, as shown in eq 13 below[49]

$$\gamma = \gamma_0 + \epsilon_o \frac{\epsilon_M\left(1 - \frac{\epsilon_M}{\epsilon_w}\right)}{2L} V^2 \tag{13}$$

Substituting eq 13 for γ in eq 12 for W_p yields the following expression for the pore formation energy

$$W_P = -\pi R_P^2 \left(\gamma_0 + \epsilon_o \frac{\epsilon_M\left(1 - \frac{\epsilon_M}{\epsilon_w}\right)}{2L} \left(\left(\frac{2\epsilon_w}{\epsilon_w + \epsilon_M} \right) \left[\frac{\xi a e^{-\kappa(d-a)}}{d} \right] \right)^2 \right) + 2\pi R_P \Gamma + \Delta\Delta H (4\pi R_P^2 \rho_n) \tag{14}$$

The final model eq 14 is consistent with several experimental observations. Specifically, (i) both positively charged and negatively charged nanoparticles are equally able to traverse the chloroplast membrane, as long as the magnitude of the surface potential, but not its sign, exceeds a certain value. This result follows from eqs 10, 12, and 13. As the zeta potential of the nanoparticle increases, the induced potential drop across the lipid bilayer also increases, as shown in eq 10. This in turn leads to a higher value of the membrane tension (see eq 13), and consequently, the work required for pore formation is reduced (see eq 12), enabling nanoparticle entry. The critical radius, r_c, can be found by setting $\frac{dW_P}{dR_P} = 0$, resulting in the following expression for r_c

$$r_c = \frac{\Gamma}{\left(\gamma_0 + \epsilon_o \frac{\epsilon_M\left(1 - \frac{\epsilon_M}{\epsilon_w}\right)}{2L} \left(\left(\frac{2\epsilon_w}{\epsilon_w + \epsilon_M} \right) \left[\frac{\xi a e^{-\kappa(d-a)}}{d} \right] \right)^2 - 4\Delta\Delta H \rho_n \right)} \tag{15}$$

The expression for the critical energy barrier $W_{P,c}$ is given by

$$W_{P,c} = \frac{\pi \Gamma^2}{\left(\gamma_0 + \epsilon_o \frac{\epsilon_M\left(1 - \frac{\epsilon_M}{\epsilon_w}\right)}{2L} \left(\left(\frac{2\epsilon_w}{\epsilon_w + \epsilon_M} \right) \left[\frac{\xi a e^{-\kappa(d-a)}}{d} \right] \right)^2 - 4\Delta\Delta H \rho_n \right)} \tag{16}$$

It then follows that when the pore radius, R_P, is less than r_c, the pore experiences an inward force that leads to the closing of the pore. On the other hand, pores with radius larger than r_c expand spontaneously. A pore forms spontaneously when R_P is larger than r_c. When a nanoparticle approaches the lipid membrane, the induced voltage causes membrane softening, which in turn leads to the formation of a pore and the nanoparticle gets completely encapsulated inside the lipid membrane. This indicates that the pore radius, R_P, corresponding to a successful nanoparticle insertion into the lipid membrane should be comparable, or larger than, the radius of the nanoparticle (i.e., $r_c \sim a < R_P$) . Setting $r_c = a$ in eq 15 results in the following expression for the nanoparticle radius, a

$$a = \frac{\Gamma}{\gamma_0 + \left(\epsilon_o \frac{\epsilon_M\left(1 - \frac{\epsilon_M}{\epsilon_w}\right)}{2L} \right) (V^*)^2 - 4\Delta\Delta H \rho_n} \tag{17}$$

where V^* is the threshold transmembrane potential drop above which a nanoparticle with radius a would be able to penetrate the lipid membrane. Equation 17 can be further simplified to obtain the following dependence of the threshold membrane potential on the nanoparticle radius

$$V^* = \pm \sqrt{\frac{\Gamma - a\gamma_0 + 4a\Delta\Delta H \rho_n}{\frac{a\epsilon_0 \epsilon_M\left(1 - \frac{\epsilon_M}{\epsilon_w}\right)}{2L}}} \tag{18}$$

Equation 10 can then be used to obtain the following expression of the threshold surface potential (ξ^*) from eq 18, required for nanoparticle penetration into the lipid membrane

$$\xi^* = \pm \left(\frac{\epsilon_M + \epsilon_w}{\epsilon_w} \right) \left(\frac{d}{a} \right) e^{\kappa(d-a)} \sqrt{\frac{(\Gamma - a\gamma_0 + 4a\Delta\Delta H \rho_n) L}{2a\epsilon_0 \epsilon_M \left(1 - \frac{\epsilon_M}{\epsilon_w}\right)}} \tag{19}$$

Equation 19 shows that ξ^* increases with increasing Γ or with decreasing γ_0. Physically, this indicates that increasing Γ or decreasing γ_0 results in an enhancement of the energy barrier for nanoparticle penetration into the lipid membrane as shown in eq 16. This enhancement in the energy barrier can only be suppressed if the nanoparticle has higher surface potential. A good fit to the observed data could be obtained using known estimates for the various parameters (Table 1). A solution to eq 19 at the asymptotic limit of $d = a$ is shown by the blue lines in Figures 1c and 3c. For nanoparticles with smaller radius, ξ^* has an inverse square root dependence on the size of the nanoparticle given by

$$\xi^* \sim \pm \left(\frac{\epsilon_M + \epsilon_w}{\epsilon_w} \right) \sqrt{\frac{\frac{\Gamma}{a} L}{2\epsilon_0 \epsilon_M \left(1 - \frac{\epsilon_M}{\epsilon_w}\right)}}$$

This indicates that nanoparticles smaller in size require a larger surface potential in order to penetrate the lipid bilayer.

Table 1. Physical Parameters Used in the LEEP Model[a]

physical parameters	approximate value	remarks
Γ	10^{-12} N[51]	
L	1.1×10^{-10} m	
γ_0	0.6×10^{-3} N/m[51]	estimated value
p_n	10^{18} m^{-2} [59]	approximate density calculated from the size of the lipid headgroup
$\Delta\Delta H$	$\sim 0.05\ k_bT$[47,50]	estimated barrier energy of binding per site on nanoparticle, assuming constant and complete lipid coverage on the nanoparticle
ϵ_M	2.2 (for chloroplast)[40]	dielectric permittivity for the chloroplast double bilayer membrane structure

[a]L is the thickness of the membrane dielectric and is utilized as a fitting parameter and bounded from 0 to 5 nm (thickness of the bilayer).

DOI: 10.1021/acs.nanolett.5b04467
Nano Lett. 2016, 16, 1161−1172

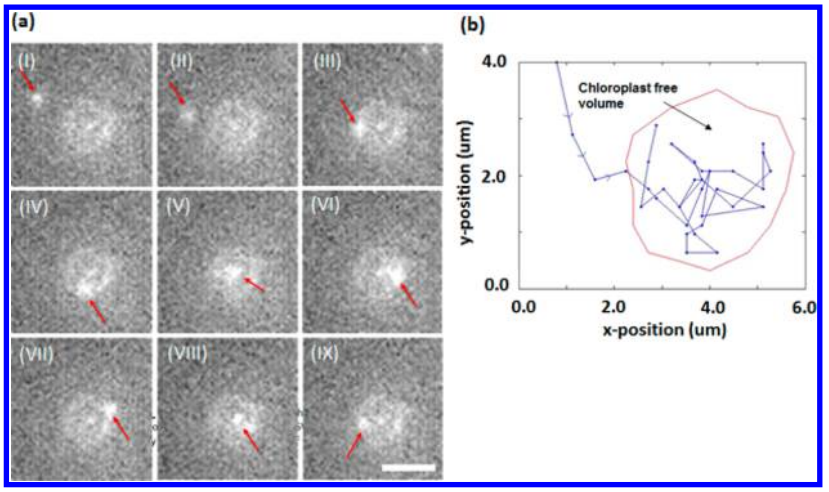

Figure 4. Representative images showing confined diffusion of SWCNTs within the chloroplast interior. (a) The tracked SWCNT (labeled by the red arrow) is observed to diffuse within the chloroplast interior, bounded by the chloroplast membrane. (b) The SWCNT path is visualized using an $x-y$ location plot, allowing the identification of the chloroplast free volume. Scale bar = 5 μm.

For larger nanoparticles, ξ^* is independent of the size of the nanoparticle and is given by

$$\xi^* \sim \pm\left(\frac{\epsilon_M + \epsilon_w}{\epsilon_w}\right)\sqrt{\frac{(4\Delta\Delta H\rho_n - \gamma_0)L}{2\epsilon_0\epsilon_M\left(1 - \frac{\epsilon_M}{\epsilon_w}\right)}}$$

The LEEP mechanistic model enables making several predictions about the nanoparticle entry into the chloroplast. First, it predicts symmetry in chloroplast entry with respect to the sign of the nanoparticle surface potential as shown in eq 18. If the absolute value of ξ^* exceeds a threshold, as defined by the model lines in Figure 3c, the nanoparticle is able to enter the chloroplast. Second, the model predicts that below a particular nanoparticle radius, entry of nanoparticles into the chloroplast requires unphysical zeta potential values. Substituting the values of the various parameters listed in Table 1 in eq 18, we find that nanoparticles of radius a = 0.5 nm require zeta potential values ξ > 80 mv in order to penetrate the lipid membrane. This accounts for the observed impermeability of the chloroplast membrane to small proteins and nucleotides (size of nucleotide ~0.34 nm).[52] In the case of neutral nanoparticles with $\xi^* \to 0$ mV, nanoparticle entry is not possible. The predictions of the LEEP model are consistent with the experimental data shown, as well as with existing knowledge of the chloroplast structure under applied stress. A variety of treatments, such as mild heat shock or charge shielding by divalent cations, can induce nonbilayer H_{II} hexagonal phase shifts in chloroplast membranes.[53] Such phase shifts also occur in an environment of low pH or when the interactions between membrane components are disrupted.[54−56] This observation is attributed to the fact that chloroplast membranes typically consist of a high proportion of galactolipids such as monogalactosyldiacylglycerol (MGDG),[57] which is a cone-shaped galactolipid that possesses highly unsaturated phospholipid tails.[58] Under environments of heat shock or low pH, the chloroplast membrane lipids assemble into hexagonal H_{II} phases, which exposes the hydrophobic surfaces toward the chloroplast exterior.[53] We postulate that the exposed lipids can then interact with the nanoparticles and facilitate their entry.

We note that the LEEP model rationalizes the effect of charge and size of the nanoparticle on a simple generalized membrane, which may be a contributing factor toward the observations of charge-mediated nanoparticle entry into mammalian cells as reported by several authors.[32,60−62] However, we would like to stress that the proposed LEEP model has some limitations. The LEEP model satisfies general principles based on surface charge, lipid affinity, and nanoparticle radius and successfully predicts the ability or inability of nanoparticles to penetrate the chloroplast. It does not, however, predict the efficiency with which nanoparticles are able to enter the chloroplast. Furthermore, to arrive at an analytical expression, we have assumed that the nanoparticles are spherical, and used the Debye−Huckel linearization of the Poisson−Boltzmann equation to calculate the electric potential profile around the charged nanoparticle. At high temperatures (above the physiological temperatures considered here), the entropic effects of lipid-nanoparticle interactions can also be significant.[63] Accounting for nanoparticle shape asymmetry would further require a numerical solution to the LEEP model. In the mathematical model, we have also not considered other variables, including membrane type (composition of lipids), ligand density on the nanoparticle, and also kinetic aspects such as incubation time. However, the aforementioned assumptions appear justified a posteriori based on the agreement between the LEEP model and the various experimental results considered.

Step 4: Kinetic Trapping of Nanoparticles. As the nanoparticle continues to move through the lipid membrane and further into the chloroplast, the induced potential at the membrane surface begins to decay. The energy required to create a pore, W_p, can be plotted against the pore size (Figure S8). W_p reaches a maximum equal to W_{pc} (the critical barrier energy) when r_c (critical radius) = a. This is shown (SI Figure S8, red line) for ξ^* = 70.2 mV (V^* = 136.7 mV) which corresponds to $r_c = a$ = 1 nm. In line with the LEEP model, nanoparticles with radii greater than, or equal to, a = 1 nm having ξ^* = 70.2 mV are able to penetrate the membrane. When these 1 nm nanoparticles continue to move further inside the membrane and become lipid wrapped, the magnitude of the induced potential at the membrane surface begins to decay resulting in a lateral shift in W_p (SI Figure S8, blue line) and to a larger value for the critical radius, $r_{c,new}$. Consequently, the pore faces a net inward force and closes because R_p = 1 nm < $r_{c,new}$. Using single-particle tracking, ss$(AT)_{15}$-SWCNTs were

DOI: 10.1021/acs.nanolett.5b04467
Nano Lett. 2016, 16, 1161−1172

found to exhibit convection and confined diffusion within the stroma space before becoming kinetically trapped. Confined diffusion of SWCNTs was observed (Figure 4 (a), and SI movie M2), with trajectories within the chloroplast shown in Figure 4 (b). The distinct free volume within the chloroplast can be characterized by tracking the confined diffusion trajectories and fitting these to an MSD curve in the form of eq 20 (where C is the corral size, and A and B are constants determined by the corral geometry).[64]

$$\mathrm{MSD}_{\mathrm{confined}} = C\left[1 - A\exp\left(-\frac{4BDt}{C}\right)\right] \quad (20)$$

Regression of the MSD curve yielded a corral size of approximately 1.6 μm^2, which is expectedly larger than that of a single chloroplast granum (0.5 μm^2).[65] In most tracked trajectories, SWCNTs which entered the chloroplast were found to eventually reach a kinetically trapped state within the chloroplast interior. Particles may be able to exit the chloroplast if they encounter surfaces that otherwise deplete lipids from the nanoparticles. However, based on our movies of SWCNTs trapped inside the chloroplast (SI movie M2), the exit of nanoparticles from the chloroplast is rare and does not occur on the time scale of the original translocation. Nanoparticles could have been trapped in the thylakoid membranes within the chloroplast, which could account for the enhanced photosynthetic efficiency of chloroplasts infiltrated particularly with SWCNTs.[9] SWCNTs that become trapped do so irreversibly, and were found to stay stationary in their 2D spatial positions until the end of the experiment, which is at a time scale far greater than that characterizing nanoparticle entry.

In summary, the mechanism of entry into and eventual trapping of nanoparticles and SWCNTs in chloroplasts was studied for the first time by confocal microscopy and by the single-particle tracking of nonphotobleaching $ss(AT)_{15}$-bound SWCNTs. SWCNTs were found to passively penetrate across the chloroplast membrane. Once in the chloroplast, SWCNTs exhibit both confined diffusion and convection, before reaching an irreversibly trapped state. We have proposed a LEEP mechanism, including formulating a LEEP model, for nanoparticle entry into the chloroplast. The LEEP mechanism/model is consistent with existing knowledge on chloroplast membrane structure as well as with our experimental findings. The model enables a physical and mathematical understanding of the effect of charges on a simple generalized membrane. Additional studies of the effect of nanoparticle orientation on its entry into chloroplast would yield further design principles that can realize the important goal of using nanoparticles as possible molecular transporters into plastids like the chloroplast.

■ ASSOCIATED CONTENT

Supporting Information

The Supporting Information is available free of charge on the ACS Publications website at DOI: 10.1021/acs.nanolett.5b04467.

Experimental details and supporting figures. (PDF)

SWCNTs trapped inside the chloroplast. (AVI)

SWCNTs trapped inside the chloroplast. (AVI)

■ AUTHOR INFORMATION

Corresponding Author

*E-mail: strano@mit.edu. Phone: 617.324.4323. Fax: 617.258.8224.

Author Contributions

The manuscript was written through contributions by M.H.W, R.P.M., J.P.G., D.B., and M.S.S. Experiments were designed and performed by M.H.W., J.P.G., and S.K. Chloroplast isolation and AFM work were done by M.H.W., S.K., Y.S., and M.P.L. The LEEP model development was written through contributions from M.H.W., R.P.M., J.W.S., D.B., and M.S.S. All authors have given approval to the final version of the manuscript.

Funding

Department of Energy (DOE); Agency of Science Technology and Research Singapore.

Notes

The authors declare no competing financial interest.

■ ACKNOWLEDGMENTS

The authors gratefully acknowledge support from the respective funding agencies. This work was entirely supported by the U.S. Department of Energy, Office of Science, Basic Energy Sciences under Award Grant DE-FG02-08ER46488 Mod 0008. W.M.H. acknowledges a graduate fellowship under the Agency of Science and Technology Singapore. M.P.L. acknowledges an NSF postdoctoral research fellowship under award no. 1306229, a Burroughs Wellcome Fund Career Award at the Scientific Interface (CASI), and a NARSAD foundation young investigator grant. The authors also wish to thank Gaurav Verma for helpful discussions.

■ ABBREVIATIONS

nIR, near-infrared; SWCNT, single-walled carbon nanotubes; $ss(AT)_{15}$, single-stranded $(AT)_{15}$ sequence DNA

■ REFERENCES

(1) Solanki, P.; Bhargava, A.; Chhipa, H.; Jain, N.; Panwar, J. *Nano-fertilizers and their smart delivery system*; Springer: New York, 2015.

(2) Liu, Z.; et al. Drug Delivery with Carbon Nanotubes for In vivo Cancer Treatment. *Cancer Res.* **2008**, *68*, 6652.

(3) Skandani, A.; AlHaik, M. Reciprocal effects of the chirality and the surface functionalization on the drug delivery permissibility of carbon nanotubes. *Soft Matter* **2013**, *9*, 11645.

(4) Svab, Z.; Hajdukiewicz, P.; Maliga, P. Stable transformation of plastids in higher plants. *Proc. Natl. Acad. Sci. U. S. A.* **1990**, *87*, 8526–8530.

(5) Ye, G.; Daniell, H.; Sanford, J. Optimization of delivery of foreign DNA into higher-plant chloroplasts. *Plant Mol. Biol.* **1990**, *15*, 809–820.

(6) Heller, D. A.; et al. Single-Walled Carbon Nanotube Spectroscopy in Live Cells: Towards Long-Term Labels and Optical Sensors. *Adv. Mater.* **2005**, *17*, 2793–2799.

(7) Heller, D. A.; et al. Optical Detection of DNA Conformational Polymorphism on Single-Walled Carbon Nanotubes. *Science* **2006**, *311*, 508–511.

(8) Lenert, A.; et al. A nanophotonic solar thermophotovoltaic device. *Nat. Nanotechnol.* **2014**, *9*, 126–130.

(9) Giraldo, J. P.; et al. Plant nanobionics approach to augment photosythesis and biochemical sensing. *Nat. Mater.* **2014**, *13*, 400–408. Giraldo, J. P.; Landry, m. P.; Kwak, S.-Y.; Jain, R. M.; Wong, M. H.; Iverson, N. M.; Ben-Naim, M.; Strano, M. S. A Ratiometric Sensor Using Single Chirality Near-Infrared Fluorescent Carbon Nanotubes: Application to In Vivo Monitoring. *Small* **2015**, *11* (32), 3973–3984.

DOI: 10.1021/acs.nanolett.5b04467
Nano Lett. 2016, 16, 1161–1172

(10) Pogodin, S.; Baulin, V. A. Can a carbon nanotube pierce through a phospholipid bilayer. *ACS Nano* **2010**, *4*, 5293−5300.
(11) Reuel, N. F.; Dupont, A.; Thouvenin, O.; Lamb, D. C.; Strano, M. S. Three dimensional tracking of carbon nanotubes in living cells. *ACS Nano* **2012**, *6*, 5420−5428.
(12) Jin, H.; Heller, D. A.; Strano, M. S. Single-Particle tracking of endocytosis and exocytosis of single-walled carbon nanotubes in NIH-3T3 Cells. *Nano Lett.* **2008**, *8*, 1577−1585.
(13) Shi Kam, N. W.; Jessop, T. C.; Wender, P. A.; Dai, H. Nanotube molecular transporters: internalization of carbon nanotube-protein conjugates into mammalian cells. *J. Am. Chem. Soc.* **2004**, *126*, 6850−6851.
(14) Rebeiz, C. A. et al. *The chloroplast: basics and applications*; Springer Science & Business Media: Dordrecht, The Netherlands, 2010.
(15) Kanevski, I.; Maliga, P.; Rhoades, D. F.; Gutteridge, S. Plastome engineering of ribulouse-1,5-Biphosphate carboxylase/oxygenase in tobacco to form a sunflower large subunit and tobacco small subunit hybrid. *Plant Physio.* **1999**, *119*, 133−142.
(16) Hanson, M. R.; Gray, B. N.; Ahner, B. A. Chloroplast transformation for engineering of photosynthesis. *J. Exp. Bot.* **2013**, *64*, 731−742.
(17) Pengelly, J. J. L.; Forster, B.; von Caemmerer, S.; Badger, M. R.; Price, G. D.; Whitney, S. M. Transplastomic integration of a cyanobacterial bicarbonate transporter into tobacco chloroplasts. *J. Exp. Bot.* **2014**, *65*, 3071−3080.
(18) Boghossian, A. A.; et al. Application of nanoparticle antioxidants to enable hyperstable chloroplasts for solar energy harvesting. *Adv. Energy Mater.* **2013**, *3*, 881−893.
(19) Bolter, B.; Soll, J. Ion channels in the outer membranes of chloroplasts and mitrochondia: open doors or regulated gates? *EMBO Journal* **2001**, *20*, 935−940.
(20) Block, M.; Douce, R.; Joyard, J.; Rolland, N. Chloroplast envelope membranes: a dynamic interface between plastids and the cytosol. *Photosynth. Res.* **2007**, *92*, 225−244.
(21) Leegood, R.; Sharkey, T.; von Caemmerer, S. *Photosynthesis: Physiology and Metabolism*; Kluwer Academic Publishers: Dordrecht, 2000; Vol. *9*, pp 137−152.
(22) Flugge, U.; Benz, R. Pore forming activity in the outer membrane of the chloroplast envelope. *FEBS Lett.* **1984**, *169*, 85−89.
(23) Stegemann, S.; Keuthe, M.; Greiner, S.; Bock, R. Horizontal transfer of chloroplast genomes between plant species. *Proc. Natl. Acad. Sci. U. S. A.* **2012**, *109*, 2434−2438.
(24) Cerutti, H.; Jagendorf, A. Movement of DNA across the chloroplast envelope: Implications for the transfer of promiscuous DNA. *Photosynth. Res.* **1995**, *46*, 329−337.
(25) Weber, G.; Monajembashi, S.; Greulich, K.; Wolfrum, J. Uptake of DNA in chloroplasts of Brassica napus facilitated by a UV-laser microbean. *Eur. J. Cell Biol.* **1989**, *49*, 73−79.
(26) Weise, S. E.; Weber, A. P. M.; Sharkey, T. D. Maltose is the major form of carbon exported the chloroplast at night. *Planta* **2004**, *218*, 474−482.
(27) Lilley, R. M.; Fitzgerald, M. P.; Rienits, K. G.; Walker, D. A. Criteria of intactness and the photosynthetic activity of spinach chloroplast preparation. *New Phytol.* **1975**, *75*, 1−10.
(28) Jin, S.; Verkman, A. S. Single particle tracking of complex diffusion in membranes: simulation and detection of barrier, raft and interaction phenomena. *J. Phys. Chem. B* **2007**, *111*, 3625−3632.
(29) Li, G.; Tang, J. X. Diffusion of actin filaments within a thin layer between two walls. *Physical Rev. E* **2004**, *69*, 1539−1543.
(30) Marshall, B. D.; Davis, V. A.; Lee, D. C.; Korgel, B. A. Rotational and translational diffusivities of Germanium nanowires. *Rheol. Acta* **2009**, *48*, 589−596.
(31) Gonzalez-Tello, P.; Camacho, F.; Blazquez, G. Density and viscosity of concentrated aqueous solutions of polyethylene glycol. *J. Chem. Eng. Data* **1994**, *39*, 611−614.
(32) Verma, A.; Stellacci, F. Effect of Surface Properties on Nanoparticle−Cell Interactions. *Small* **2010**, *6*, 12−21.
(33) Lin, J.; Alexander-Katz, A. Cell Membranes Open "Doors" for Cationic Nanoparticles/Biomolecules: Insights into Uptake Kinetics. *ACS Nano* **2013**, *7*, 10799−10808.
(34) Hong, S.; et al. Interaction of poly (amidoamine) dendrimers with supported lipid bilayers and cells: hole formation and the relation to transport. *Bioconjugate Chem.* **2004**, *15*, 774.
(35) Hong, S.; et al. Interaction of Polycationic Polymers with Supported Lipid Bilayers and Cells: Nanoscale Hole Formation and Enhanced Membrane Permeability. *Bioconjugate Chem.* **2006**, *17*, 728.
(36) Mecke, A.; Majoros, I.-J.; Patri, A. K.; Baker, J.; Holl, M. M. B. Direct observation of lipid bilayer disruption by poly(amidoamine) dendrimers. *Chem. Phys. Lipids* **2004**, *132*, 3−14.
(37) Li, H.; Chiu, C. Protein transport into chloroplasts. *Annu. Rev. Plant Biol.* **2010**, *61*, 157−180.
(38) Loeb, A. L.; Overbeek, J. T. G.; Wiersema, P. H. *The electrical double layer around a spherical colloidal particle*; MIT Press: Cambridge, 1961.
(39) White, L. R. Approximate analytic solution of the Poisson-Boltzmann equation for a spherical colloidal particle. *J. Chem. Soc., Faraday Trans. 2* **1977**, *73*, 577.
(40) Fettiplace, R.; Andrews, D.; Haydon, A. The thickness, composition and structure of some lipid bilayers and natural membranes. *J. Membr. Biol.* **1971**, *5*, 277−296.
(41) Jackson, J. D. *Classical Electrodynamics*; Wiley: New York, 1998.
(42) Onsager, L.; Samaras, N. N. T. The surface tension of Debye-Huckel electrolytes. *J. Chem. Phys.* **1934**, *2*, 528.
(43) Bisker, G.; et al. Protein targeted corona phase molecular recognition. *Nat. Commun.* **2016**, *7*, 10241.
(44) Sikor, M.; et al. Interaction of a charged polymer with zwitterionic lipid vesicles. *Langmuir* **2010**, *26*, 4095−4102.
(45) Georgiev, G.; Sarker, D.; Al-Hanbali, O.; Georgiev, G. D.; Lalchev, Z. Effects of poly (ethylene glycol) chains conformational transition on the properties of mixed DMPC/DMPE-PEG thin liquid films and monolayers. *Colloids Surf., B* **2007**, *59*, 184−193.
(46) Langecker, M.; Arnaut, V.; List, J.; Simmel, F. C. DNA nanostructures interacting with lipid bilayer membranes. *Acc. Chem. Res.* **2014**, *47*, 1807−1815.
(47) Wang, B.; Zhang, L.; Bae, S.-C.; Granick, S. Nanoparticle-induced surface reconstruction of phospholipid membranes. *Proc. Natl. Acad. Sci. U. S. A.* **2008**, *105*, 18171−18175.
(48) Litster, J. D. Stability of lipid bilayers and red blood cell membranes. *Phys. Lett. A* **1975**, *53*, 193−194.
(49) Weaver, J. C.; M, R. A. Decreased bilayer stability due to transmembrane potentials. *Phys. Lett. A* **1981**, *86*, 57−59.
(50) Heikkila, E.; et al. Cationic Au Nanoparticle Binding with Plasma Membrane-like Lipid Bilayers: Potential Mechanism for Spontaneous Permeation to Cells Revealed by Atomistic Simulations. *J. Phys. Chem. C* **2014**, *118*, 11131−11141.
(51) Zimmermann, U. *Electromanipulation of cells*; CRC Press: Boca Raton, 1996.
(52) Watson, J.; Crick, F. A structure for deoxyribose nuclei acid. *Nature* **1953**, *171*, 737−738.
(53) Lee, A. G. Membrane lipids: It's only a phase. *Curr. Biol.* **2000**, *10*, 377−380.
(54) Carter, D. P.; Staehelin, L. A. Proteolysis of chloroplast thylakoid membranes II. *Arch. Biochem. Biophys.* **1980**, *200*, 374−386.
(55) Gounaris, K.; Brain, R.; Quinn, J.; Williams, P. Structural reorganisation of chloroplast thylakoid membranes in response to heat stress. *Biochim. Biophys. Acta, Bioenerg.* **1984**, *766*, 198−208.
(56) Williams, W. P.; Quinn, P. J. The phase behaviour of lipids in photosynthetic membranes. *J. Bioenerg. Biomembr.* **1987**, *19*, 605−624.
(57) Joyard, J.; Ferro, M.; Masselon, C.; Seigneurin-Berny, D.; Salvi, D.; Garin, J.; Rolland, N. Chloroplast proteomics highlights the subcellular compartmentation of lipid metabolism. *Prog. Lipid Res.* **2010**, *49*, 128−158.
(58) Block, M. A.; Jouhet, J.; Marechal, E.; Bastien, O.; Joyard, J. *Photosynthesis: Plastid biology, energy conversion and carbon assimilation*; Springer Science: Dordrecht, 2011.

DOI: 10.1021/acs.nanolett.5b04467
Nano Lett. 2016, 16, 1161−1172

(59) Kupiainen, M.; Falck, E.; Ollila, S.; Niemela, P.; Gurtovenko, A. Free volume properties of sphingomyelin, DMPC, DPPC, and PLPC Bilayers. *J. Comput. Theor. Nanosci.* **2005**, *2*, 401−413.
(60) Chen, L.; Mccrate, J.; Lee, J.; Li, H. The role of surface charge on the uptake and biocompatibility of hydroxyapatite nanoparticles with osteoblast cells. *Nanotechnology* **2011**, *22*, 105708.
(61) Liu, B. et al. *Effects of surface charge and particle size of cell-penetrating peptide/nanoparticle complexes on cellular internalization*; Nova Science Publishers Inc.: Hauppauge, NY, 2013.
(62) Villanueva, A. The influence of surface functionalization on the enhanced internalization of magnetic nanoparticles in cancer cells. *Nanotechnology* **2009**, *20*, 115103.
(63) Farago, O.; Santangelo, C. Pore formation in fluctuating membrane. *J. Chem. Phys.* **2005**, *122*, 044901.
(64) Saxton, M. J. Single-Particle Tracking: Effects of Corrals. *Biophys. J.* **1995**, *69*, 389−398.
(65) Consoli, E.; Croce, R.; Dunlap, D. D.; Finzi, L. Diffusion of light-harvesting complex II in the thylakoid membranes. *EMBO Rep.* **2005**, *6*, 782−786.

■ NOTE ADDED AFTER ASAP PUBLICATION

This paper was published on the Web on January 26, 2016. Additional corrections were made to column 2 of Table 1, and the corrected version was reposted on February 1, 2016.

DOI: 10.1021/acs.nanolett.5b04467
Nano Lett. 2016, 16, 1161−1172